PLANETARY SCIENCE

Freeze-thaw cycles drove chemical weathering and enriched sulfates in the Burns formation at Meridiani, Mars

Jiacheng Liu[1,2], Joseph R. Michalski[1,2]*, Wenyuan Gao[3], Christian Schröder[4], Yi-Liang Li[1]

Sulfate-rich sedimentary rocks explored by the Opportunity rover during its 14-year surface mission at Meridiani Planum provide an invaluable window into the thousands of sulfate deposits detected on Mars via remote sensing. Existing models explaining the formation of martian sulfates can be generally described as either bottom-up, groundwater-driven playa settings or top-down icy chemical weathering environments. Here, we propose a hybrid model involving both bottom-up and top-down processes driven by freeze-thaw cycles. Freezing leads to cryo-concentration of acidic fluids from precipitations at the surface, facilitating rapid chemical weathering despite low temperatures. Cryosuction causes the upward migration of vadose water and even groundwater with dissolved ions, resulting in the accumulation of ions in near-surface environments. Evaporation precipitates salts, but leaching separates chlorides from sulfates during the thawing period. Freeze-thaw cycles, therefore, can enrich sulfates at the surface. While freeze-thaw is more commonly understood as a mechanism of physical weathering, we suggest that it is a fundamental aspect of chemical weathering on Mars.

INTRODUCTION

The mechanism by which widespread sulfates formed during the Hesperian (~3 to 3.7 billion years ago) remains an unresolved aspect of Mars' geologic history with great implications for past climate, fundamental sedimentary processes, and astrobiology (*1*–*8*). Although sulfates on Earth are often found in evaporitic lacustrine or marine settings, very few candidate lacustrine basins on Mars are associated with sulfates (*9*–*11*). Martian sulfates detected via infrared remote sensing are found in a range of environments and elevations from dunes in the high northern latitudes to several kilometer–high sedimentary mounds within craters or parts of the Valles Marineris canyon system (*1*–*8*, *12*), but most of the deposits occur in near-equatorial layered deposits of enigmatic origins (*13*–*15*), especially at Meridiani Planum.

The Opportunity rover was sent to Meridiani Planum to investigate a remotely sensed infrared signature of hematite (*16*, *17*). Rover data revealed that the Fe oxides co-occur with sulfate in layered sedimentary rocks (*18*). Mineralogical, geochemical, textural, and stratigraphic data returned from the rover over 45 km of horizontal space, and tens of meters of stratigraphic section provided a wealth of geological information about the sedimentary rocks at Meridiani and provided fundamental ground truth about remotely detected martian sulfates applicable to the rest of Mars. The rich datasets returned from Opportunity, especially collected from the Burns formation, led to proposals of multiple models to explain the formation of sulfates in that setting, and these models can be grouped into groundwater upwelling/playa hypotheses (*19*–*24*) and icy weathering/top-down concepts (*5*, *8*, *25*), although several other ideas have also been suggested (*18*, *26*–*28*). The playa/upwelling versus icy weathering/top-down models have very different implications for the ancient martian climate. For the formation of the regional layered sulfate-rich sediments (*29*), a playa environment suggests a long-lived global groundwater system (*22*, *23*). It indicates a long-term warm climate with a large total water inventory on early Mars (*22*). In contrast, the icy weathering model proposes that the Meridiani sedimentary deposits are the result of eolian/impact-driven reworking of the sublimation residue from a large-scale eolian dust and ice deposit (*5*, *8*). It implies that icy and dry environments may have been typical on early Mars (*30*).

The groundwater upwelling scenario is largely embraced because modeling of martian global hydrology suggests that Meridiani Planum is among the regions with the shallowest predicted water table on Mars (*23*). Liquid water to facilitate weathering is a critical constraint on any model, and groundwater predictions provide a mechanism to deliver liquid water to perform alteration, at least in some of the physiographic or topographic settings. The upward transport of groundwater during diagenesis can also potentially explain a progressive enrichment of sulfates higher in the Burns formation (*24*, *29*, *31*, *32*). A problem with this model is that it predicts that upwelling should occur in many locations where sulfates or comparable sedimentary geology is not observed (*9*–*11*, *23*). Another potential challenge is that it is not clear how the standard model of groundwater upwelling in playas could explain the low water/rock ratios indicated by the ubiquitous jarosite in the Burns formation at Meridiani Planum (*8*). Last, the scenario needs to address the issue of the amount of CO_2 sequestration by the subsurface formation of carbonate during global groundwater circulation (*33*).

As an alternative, the icy weathering model suggests that the water-limited, acidic environment can be created by freezing within large-scale, homogeneous, eolian deposits (*5*, *30*), which can explain its large distribution area and compositional similarity of the Burns formation (*8*). The icy weathering model is further supported by the elevated weathering rate of olivine under icy temperatures (*30*, *34*) and a recent discovery of authigenic jarosite in deep Antarctic ice (*35*). Top-down, icy weathering can potentially explain the formation of sulfates as draping sedimentary deposits at any elevation and in many contexts including mounds (*5*) and does not suggest that sulfates should form in topographic basins. Although an icy weathering model (*5*, *8*, *30*) has many advantages, it does not explain

[1]Department of Earth Sciences, the University of Hong Kong, Hong Kong. [2]Laboratory for Space Research, the University of Hong Kong, Hong Kong. [3]Department of Geology, Northeastern University, Shenyang, China. [4]Biological and Environmental Sciences, University of Stirling, Stirling, FK9 4LA, UK.
*Corresponding author. Email: jmichal@hku.hk

rock textures (e.g., diagenetic nodules, pore-filling cements, and secondary porosity) considered a central advantage to the playa-diagenesis models (*32*).

Here, we propose a hybrid freeze-thaw cycling scenario, driven by icy weathering and facilitated by communication with a local or regional, shallow groundwater source. Freeze-thaw is a fundamental geologic process on any liquid water–bearing planet with temperatures near 0°C, and we propose that this simple aspect of the martian geosystem is essential to its geochemical and hydrological cycling. On Earth, freeze-thaw cycles can cause strong salinization of soils (*36*) and the formation of hematite spherules (*37*, *38*). Freezing of the surface and the near-surface concentrates H_2O from surface, atmospheric sources, and the subsurface, inducing upward migration of shallow groundwater by cryosuction. Note that even in high-elevation (~2800 m), cold deserts such as in the Qaidam Basin (fig. S1) where a global groundwater system is not possible, regional snowmelt (*39*) is sufficient to recharge local, shallow groundwater flow driving freeze-thaw processes (*40*).

Effects of cryosuction are stronger in fine-grained (e.g., silt-sized) materials (*41*) and theoretically higher at lower gravity on Mars. Here, we propose a seasonal freeze-thaw model that combines the strengths of both groundwater and icy weathering scenarios and can thus explain most phenomena and measurements in the Burns formation at Meridiani. Water cycling through capillary action in freeze-thaw conditions might be a fundamental process affecting all surface environments on Mars.

RESULTS AND DISCUSSION

Evidence for freeze-thaw cycles

The stratigraphy revealed by impact craters (e.g., Endurance, Victoria, and Endeavour craters) at Meridiani Planum provides an invaluable window into geochemical and textural trends in the sulfate-rich bedrock (*24*, *29*, *42*, *43*). The lowermost and oldest layers at Meridiani corresponding to the Noachian Matijevic formation predate the Endeavour impact (*44*, *45*). This formation is overlain by the Shoemaker formation, the Grasberg formation, and the Burns formation (fig. S2) (*44*–*46*). The Grasberg formation has been subdivided into a lower dark-toned unit and an upper light-toned, polygonally fractured unit (fig. S3) (*44*, *46*). The sediment grains of both subunits of the Grasberg bedrock are too small to be resolved by the Microscopic Imager (MI) onboard Opportunity (*46*) (i.e., <100 μm). The Burns formation can be divided into three units (Fig. 1, A and B) (*24*): the lower cross-laminated sediments interpreted as a dry dune field (*24*); the middle horizontally laminated layers rich in 3- to 5-mm hematite spherules, interpreted as an eolian sand sheet and interdune playa (*24*); and an upper, high-albedo, brecciated unit, the bedding of which were substantially disrupted (Fig. 1, A to C). The sand grains in the Burns formation are aggregates of sulfates and siliciclastic components (Fig. 1, D and E) (*19*, *21*, *24*, *32*). The formation of the eolian sand sheet in the middle unit of the Burns formation may be related to a high water table (*24*, *47*).

Although the Grasberg and Burns formations differ in terms of their grain size and textures (Fig. 1A and fig. S3), their uppermost parts are similar with regard to their brecciation and albedo (fig. S2, B to D). In addition, the coupling of a lower dark zone to an upper bleached and brecciated zone seen in Endurance (Fig. 1B) is notably similar to the coupled units observed later in the mission in Victoria crater (Fig. 1C) (*25*). The brecciation and the albedo sequences appear in different locations, elevations, and stratigraphic positions (*25*), so it is likely that these trends are linked to the topographic surface not the stratigraphy itself. Although brecciation observed in cross sections within and around impact craters could have been caused by the impact events themselves (*19*, *20*, *48*), the brecciation is also observed in surface rocks throughout the region beyond those exposed in the craters (*49*). In addition, the albedo positively correlates with the degree of brecciation and expansion, both of which decrease quickly from the upper units to the middle/lower units (Fig. 1, A to C). It suggests that the high albedo and brecciation are geologically linked. Acidic bleaching has been suggested to account for the high albedo in the Burns formation (*50*). We suggest that seasonal freeze-thaw cycles, which can happen cyclically on the surface, can account for the coupled existence of brecciation and bleaching. The brecciation and the disruption of bedding may be the result of cryogenic expansion, and the bleaching was caused by icy acidic leaching. The horizontal boundary between the upper bleached unit and the lower dark unit (Fig. 1, A to C) suggests the location of the ancient frozen front.

The porosity in the Burns formation is high (*32*). The high porosity does not stem from fine voids but mainly from two types of large voids (centimeter long) in sediments: vugs with tapered edges (Fig. 1D) (*19*, *32*) and sheet-like vugs (Fig. 1E) (*32*). Vugs with tapered edges (Fig. 1D), observed over about 5% of the outcrop at Meridiani Planum (*19*, *32*), are interpreted as crystal molds, which are similar in shape to the crystal habit of meridianiite ($MgSO_4{\cdot}11H_2O$) (*51*). Meridianiite is stable below 2°C and generally exists in ice or a frozen zone (*52*). When the temperature rises above 2°C, meridianiite decomposes into epsomite ($MgSO_4{\cdot}7H_2O$) and water (*51*, *52*). The widespread euhedral meridianiite crystal–like molds, therefore, imply temperature fluctuation around 2°C happened in the Burns formation.

The Burns formation also exhibits sheet-like vugs that are separated by sediment aggregates resembling stacks of wavy plates (Fig. 1E). The platy structure with large planar voids but few fine voids can be attributed to freeze-thaw cycles (*53*–*55*). During the freezing stage, water accumulated in voids expands volumetrically and enlarges the voids. As growing ice crystals exert pressure on the matrix surfaces, the freeze-thaw cycles can increase the number of coarse voids but result in a marked reduction in the number of fine voids (*56*). This process leads to condensation and aggregation of sediments (*57*). The horizontal development of ice crystal and ice lenses during freeze-thaw cycles elongates the sediment aggregates horizontally (*54*), which explains the observed platy structure in the Burns formation (Fig. 1E).

The large voids can provide space for the crystallization of sulfates, such as meridianiite, which can shape the void further owing to the growth and expansion of salt crystals. Meridianiite can form and decompose in each single freeze-thaw cycle as a result of temperature fluctuations. Therefore, the size of the void and the size of the meridianiite crystals can increase with number of freeze-thaw cycles. When there is sufficient space for salt crystallization, the size of meridianiite crystals can reach centimeter scale (*52*).

The highly similar chemical composition for the Grasberg and Burns formations suggests that the sands in the Burns formation may originate from Grasberg-like precursor (*46*, *58*). The freeze-thaw cycles and/or icy weathering can cause the initial formation of sulfate minerals (*8*) in the Grasberg formation, which indurated its fine-grained materials. Through aeolian processes, the erosion and rework of the upper part of the indurated deposits, consisting of a

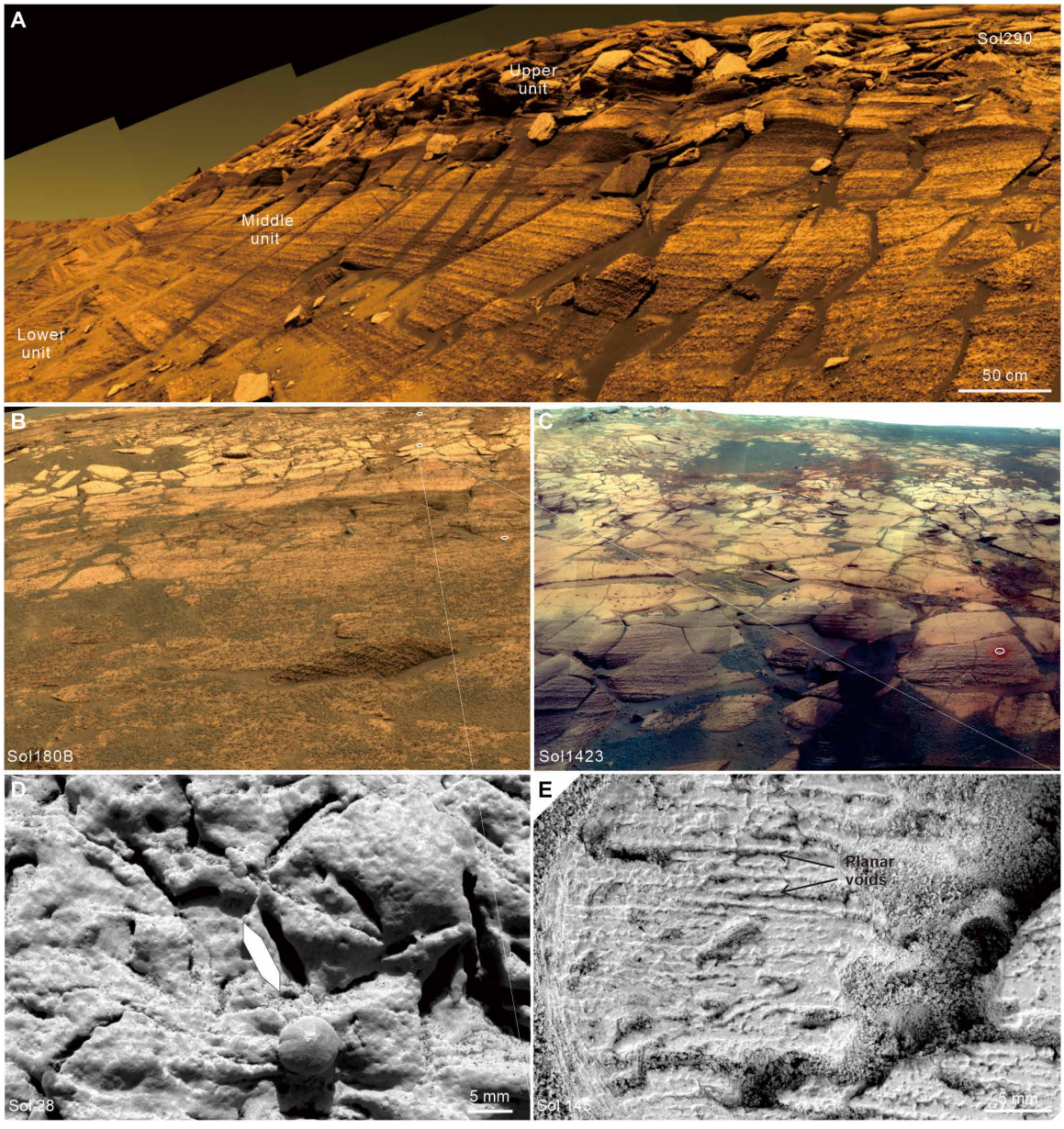

Fig. 1. Geological features in the Burns formation that may reflect freeze-thaw cycles. (**A**) Intensive brecciation and expansion of sedimentary blocks of the upper unit of the Burns formation at Endurance crater (PIA07110). (**B** and **C**) Sequences with upper bleaching and brecciated zone and lower darker and less brecciated zone at Endurance crater (P2406) (B) and Victoria crater (P2419) (C), respectively. (**D**) The plate-shaped voids with tapered edges that are similar to the crystal morphology of Meridianiite. The image is part of the MI mosaic of outcrop surface (McKittrick). (**E**) Stacks of wavy plates separated by planar voids. The image is part of a mosaic of abraded outcrop surface (Cobble Hill). The size of the APXS spot represented by white circles is 38 mm in diameter. Image credit: NASA/JPL-Caltech.

mixture of sulfate minerals and fine-grained siliciclastics, can provide the source for the deposition of the Burns formation and explain the regional homogeneity of sediments in Burns formation. The deepest materials remained in place and eventually became the Grasberg formation. In the Burns formation, further freeze-thaw cycles can lead to the condensation and aggregation (*54*) of the mixture of sulfate minerals and fine-grained siliciclastics (Fig. 1D and E).

To conclude, the freeze-thaw scenario can effectively account for both macroscopic and microscopic textures of the Burns formation (Table 1), as well as the stratigraphic relationship between the Grasberg and Burns formations. Temperature fluctuations and seasonal freeze-thaw cycles near the equator were likely achievable when obliquity and eccentricity are high and when perihelion occurs near the equinox (*13*).

The sources of sulfur for the formation of sulfate-rich sediments at Meridiani

For the rock samples without veins or spherules from the Burns and Grasberg formations (152 measurements), there are good correlations between Al and Si ($R^2 = 0.84$; Fig. 2A) and between Al and Ti ($R^2 = 0.56$; Fig. 2B) based on chemical results from the alpha-particle x-ray spectrometer (APXS). The high porosity of the Burns sediments

Table 1. Characteristics of sedimentary deposits of the Burns formation at Meridiani and their explanation by a seasonal freeze-thaw model.

Characteristics	Processes during freeze-thaw cycles
Regional compositional similarity	Freeze-thaw cycles and aeolian activities are regional processes.
Sulfate-cemented siliciclastic nature of the sand grains	Freeze-thaw cycles produced sulfates that indurated the fine-grained dust deposits, which were eroded into sand-sized particles, that were reworked and redeposited by aeolian processes to form the sediments of the Burns formation with bedding feature.
Bedding features of the Burns rocks	
Trace olivine in rock samples	Alteration of olivine by icy acidic weathering during the freezing period.
Abundant secondary silica	Alteration of olivine can release abundant silica, the solubility of which is low in saline fluid film during freezing.
Formation of jarosite	Oxidizing and acidic conditions near the surface during the freezing period.
Stability of jarosite	Low water-rock ratios during any single freeze-thaw cycle.
High abundance of sulfates (~20%)	Salinization of sediments by 10^4 to 10^5 years of seasonal freeze-thaw cycles.
Hematite spherules	Cyclical interaction between oxidizing surface water and reducing groundwater in sediments with high porosity.
Intense brecciation in place	Cryogenic brecciation and expansion.
Bleached zone	Dissolution of nano-sized Fe(III) oxides by very acidic water generated through freezing.
Meridianiite	Freezing concentrates Mg and SO_4^{2-} under subzero temperatures.
Vugs with crystal mold	Dissolution of meridianiite during the thawing stage.
The high porosity of sediments	Cyclical ice expansion and leaching of some salts.
Upward enrichment of S, Br, and Mg	Upward migration of groundwater during freezing and precipitation of sulfates by evaporation during thawing.
Upward enrichment of Fe	Oxidation of upward migration of groundwater by near-surface oxidants (e.g., chlorates).
Upward decrease in Cl	Preferential leaching of chlorides over sulfates during thawing.
Anomalously high Br/Cl ratios	Precipitation of jarosite, which has high Br/Cl ratios.

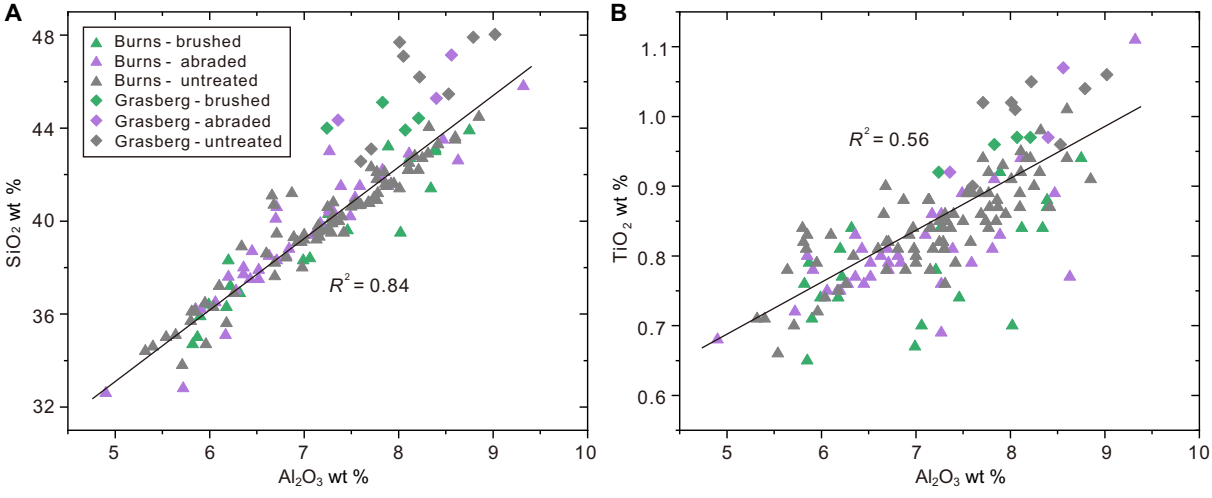

Fig. 2. The immobility of Al, Si, and Ti during alteration in the Burns and Grasberg formations. A strong correlation between Al and Si (**A**), as well as a good correlation between Al and Ti (**B**), indicating that Al, Si, and Ti are immobile in rock samples from the Burns and Grasberg formations. Soils and samples containing veins or spherules are excluded from the dataset. The error bars are smaller than or similar to the size of the data points.

(*32*) implies that the positive correlation between Al and Si is not a result of their synchronous addition. Instead, these good correlations indicate the immobility of Al and Si. The immobility of Al and Si has previously been suggested by the limited variation in the ratios of Al and Si to Ti as a function of relative stratigraphic depth (*25*, *43*, *58*). Similar immobility of Al and Si is also observed in Gale crater (*59*).

The immobility of Al in the Burns and Grasberg formations allows the ratios of other elements to Al to be used to identify the chemical behaviors of other elements during alteration. Two fundamental chemical processes are suggested in the plot of molar S/Al to molar (Mg + Ca + Fe)/Al (Fig. 3), which can identify whether sulfur was added with cations or not during alteration (*60*, *61*). From the

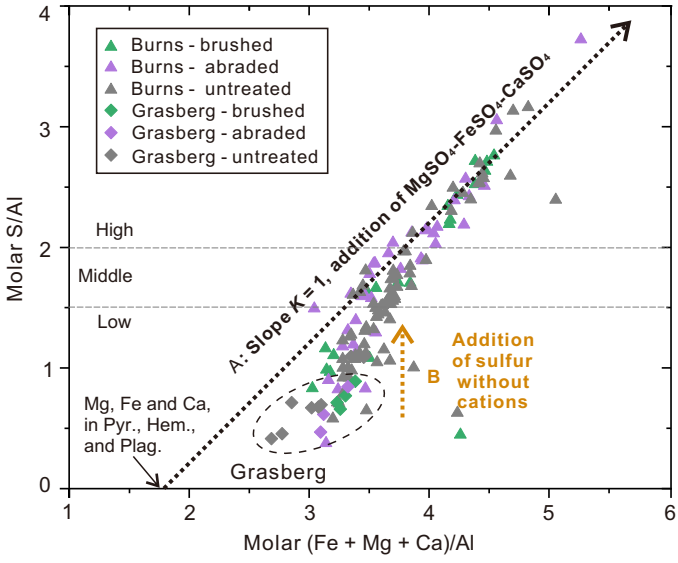

Fig. 3. The sources of the sulfur in the Burns and Grasberg formations. Arrow A, with a slope of 1, indicates the addition of sulfur along with cations with a molar ratio of S:cations equal to 1. The intersection of arrow A and with the *x* axis represents the contribution of Mg, Fe, and Ca from hematite, pyroxene, and plagioclase. Arrow B, parallel to the *y* axis, indicates the direct addition of sulfur without cations, resulting from the interaction between sulfuric acid and olivine. The trend observed in samples with low molar S/Al ratios transitioning to those with middle ratios lie between arrow A and arrow B, suggesting an additional sulfur contribution beyond the (Mg-Fe-Ca)-SO_4 addition during the initial stage of rock alteration. However, samples with middle and high molar S/Al ratios predominantly align with arrow A, indicating that the addition of (Mg-Fe-Ca)-SO_4 is the primary process during the intense stage of alteration of rock samples. Soils and samples with veins or spherules are excluded from the dataset. Error bars are smaller than or comparable to the size of the data points.

Grasberg rocks to the Burns rocks with low molar S/Al ratios, the increased values of molar S/Al are larger than the increased values of molar (Mg + Ca + Fe)/Al (Fig. 3). This suggests that additional sulfur has been enriched (arrow B), except for direct addition of sulfate with cations (arrow A). The two chemical weathering processes are consistent with the hybrid scenarios during diagenesis proposed by McCollom and Hynek (*58*). Their modeling work shows that the transformation from the Grasberg rocks to the Burns rocks requires a MgO:SO_3 ratio equal to 0.65 (2023), suggesting that ~35% sulfur was added to the Burns formation without Mg. Most of the additional sulfur may have been enriched through acidic alteration of olivine by a sulfuric acid–rich, low-pH fluid (*62*), as indicated by the widespread existence of jarosite and trace olivine in rock samples at Meridiani Planum (*32*, *63*).

Both of the two processes are suggested from the Burns rocks with low molar S/Al ratios to those with middle ratios (Fig. 3). This suggests that direct addition of sulfur and acidic weathering of silicates still exert a notable control on the chemical composition during the initial-stage alteration of the Burns rocks. For the sediments with middle and high molar S/Al ratios, their spots are nearly along the $MgSO_4$-$CaSO_4$-$FeSO_4$ sulfates line (slope $K = 1$) (Fig. 3). The trend implies a direct addition of sulfate with cations to the Burns rocks.

With the gradual consumption of the easily altered silicates by sulfuric acid during freeze-thaw cycles, the efficiency of the reaction between the sulfuric acid and the sediments decreases gradually. In the intensive alteration stage of the Burns rocks, sulfur is dominantly sourced with cations from groundwater (Fig. 3). The observations suggest that most sulfur in the Burns rocks was enriched with cations, although there is an important contribution from the sulfuric acid–rich, low-pH fluid in the initial stage of chemical alteration.

The weight ratio of elements to Al in the Burns formation suggests an upward enrichment of Mg, S, and Br but a downward enrichment of Cl in the Burns formation (Fig. 4). These trends have been previously noted (*25*, *29*, *43*), and the concurrent upward enrichment of Mg and S has been explained by groundwater upwelling scenarios involving diagenesis and evaporation (*24*, *32*, *43*). In addition, the upward accumulation of water-soluble cations (Na^+, K^+, and Ca^{2+}) and anions (Cl^-, SO_4^{2-}, and NO_3^-) has also been observed in permafrost environments such as in Wright Valley, Antarctica (*64*). However, there is no leaching trend of Cl or upward enrichment of Mg (*64*), which is different from the observations in the Burns formation. The lack of a leaching trend is because the existence of the permanently frozen zone leads to a lack of communication between the surface water and groundwater.

On the other hand, the upward depletion of Cl with upward enrichment of sulfur has been observed in hyperarid Atacama Desert soils of northern Chile (*25*, *65*). The trends have been explained by the surficial addition of S, Cl, and Br, followed by the leaching of more soluble chlorides through precipitation and the retention of less soluble sulfates. However, the hyperarid desert scenario struggles to explain the upward enrichment of Mg alongside S, the precipitation and decomposition of meridianiite, (*19*, *32*), and the formation of hematite spherules. In summary, while some chemical observations from the Burns formation can be explained by permafrost and hyperarid desert environments on Earth, there are still differences that highlight the unique conditions and processes that took place at Meridiani, Mars.

A seasonal freeze-thaw model at Meridiani

Acidic weathering and upward movement of groundwater by cryosuction

The acidity of surface water (*66*–*68*) on early Mars was driven by the atmospheric deposition of volcanogenic sulfuric/hydrochloric acid (*5*) and the hydrolysis and oxidation of aqueous Fe^{2+} by photochemistry (*69*). Photochemistry (*70*) and electrochemistry during sand/dust storms (*71*) could have formed some oxyhalogens (*72*) (e.g., chlorate) on early Mars. The oxyhalogens formed in the atmosphere can be transported to the surface by their adsorption on fine-grained particles and later air-fall sedimentation of these particles (Fig. 5A) (*70*).

Although only a smaller portion of S and Cl in the Burns formation originates from the atmosphere, the atmospheric S and Cl play an important role in the acidic and oxidizing alteration in the near surface. As the oxyhalogens dissolve rapidly in aqueous fluids, the rainwater precipitated at the surface becomes oxidizing (*73*). Freezing can counterintuitively increase the kinetics of chemical weathering because it raises the acidity and salinity of residual water (*30*). The acidic weathering also leads to the alteration of olivine to form Fe-Mg sulfates (*30*). The released Fe^{2+} can be oxidized and combined with sulfate to form jarosite (*74*) under such a cold, acidic, and oxidizing environment (*75*). The jarosite can host Br and Cl with high Br/Cl ratios (*76*). The released Si from the alteration of olivine can be precipitated as secondary silica efficiently because the solubility of Si is low in low-temperature (*77*) and saline fluids (*78*). The precipitation mechanism of silica explains the immobility of Si (Fig. 2A) and the

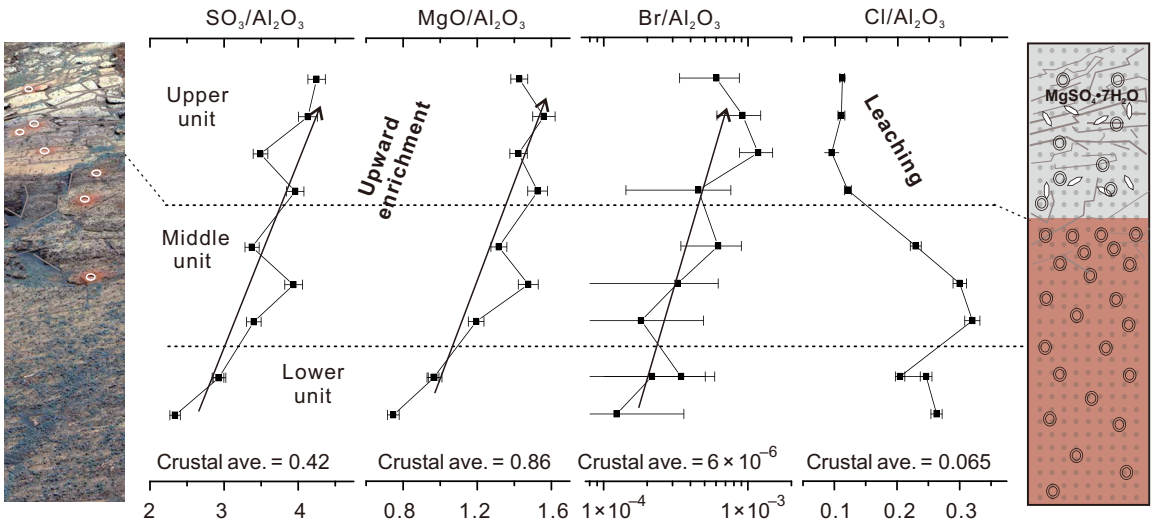

Fig. 4. Geochemical evidence for upward migration of water and sudden leaching during freeze-thaw cycles in the Burns formation. Upward enrichment in S, Mg, and Br but downward leaching of Cl indicated by their weight ratios to immobile Al. All of these ratios exceed those of their crustal averages (*87*). Sample depths are not to scale but relative and plotted at intervals defined by McCollom (*43*). The size of the APXS spot, represented by white circles, is 38 mm in diameter. The error bars shown for the ratios were calculated based on the method recommended by Dunlap and Silver (*88*).

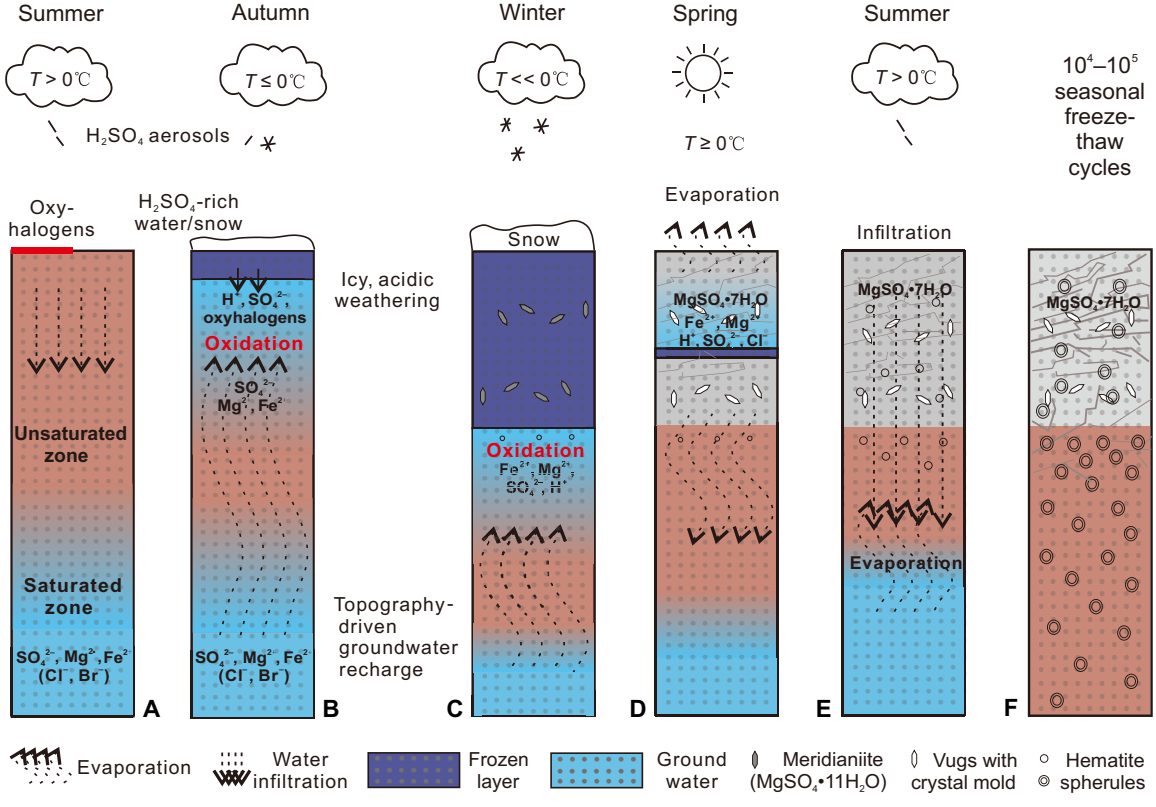

Fig. 5. A freeze-thaw model for the alteration in the Burns formation at Meridiani. (**A**) Precipitation of sulfur-bearing, acidic water, and deposition of oxyhalogen-coated sands at the surface. (**B**) As the temperature decreases, acidity concentrates during freezing of surface water, and cryosuction drives the upward movement of water and its solutes from the unsaturated and/or saturated zones. (**C**) With further temperature reduction, more groundwater and salts migrate upward to form a thick frozen zone with icy weathering of olivine and the formation of sulfates (e.g., meridianiite and jarosite). (**D**) During the thawing stage, meridianiite dissociates but other sulfates precipitate owing to evaporation. (**E**) Infiltration of unfrozen water rich in Cl occurs after the blocked pores reconnected with the thawing of ice layer. (**F**) Cycles of freeze-thaw lead to the enrichment of sulfates, formation of hematite spherules, and bleaching and fragmentation of the near-surface sediments.

high abundance of secondary silica in the rocks of the Burns formation (*32*).

Below the frozen zone, there is a vadose zone overlaying a saturated zone (Fig. 5B). As the frozen zone grows, freezing decreases available liquid water at the freezing front and creates negative pressure in the unsaturated zone (*79*). This leads to cryosuction, which results in capillary migration of vadose water upward from the groundwater source (Fig. 5B). When the initial water table is shallow, freezing-induced groundwater migration from the saturated zone could be substantial (*79*). In such case, the effect of the upward migration of water may be comparable to that of groundwater upwelling while being a fundamentally different geologic process.

Ions, including SO_4^{2-}, Cl^-, and Mg^{2+}, move upward with the migration of groundwater, which accumulates just below the frozen zone (Fig. 5B). The increasing salinity just below the frozen zone lowers the freezing point of the aqueous fluid up to 40°C (*30*). Gradual seasonal cooling leads to the formation of an interlayer liquid water zone. The further freezing of the salty water in the interlayer water zone or between grains leads to the precipitation of sulfates, such as meridianiite (Fig. 5C). Considering the high average S/Cl ratio (>3) (*80*) of martian crust and therefore groundwater, more sulfur than chlorine can migrate toward the surface.

Enrichment of sulfates but leaching of chloride

In the spring season, the increasing temperature (>0°C) leads to the gradual thaw of surface snow and the near-surface frozen zone and the decomposition and dissolution of salts precipitated during freezing, such as meridianiite. The meltwater is enough to dissolve the salts precipitated during the freezing period and the salts formed by the decomposition of meridianiite. The vugs with tapered edges similar to meridianiite crystal can form and are not filled.

As the frozen layer melts from top to down, any meltwater would presumably pond on top of the frozen layer. However, without the protection of the top frozen layer during the thawing period, surface evaporation becomes very efficient in a low-pressure (low humidity) martian environment. This promotes salt precipitation again in the upper part of sediment sequences (Fig. 5D). Before complete evaporation of surface water and precipitation of all ions as salts, the increasing temperature from spring to summer can lead to the complete thaw of the frozen zone. The blocked pores are connected again, allowing for the infiltration of the meltwater (Fig. 5E). Because of the ~37% higher solubility of NaCl compared to $MgSO_4$ at 0°C, more chlorides can dissolve and migrate downward with meltwater during the thawing periods. The freeze-thaw cycles can therefore explain the upward enrichment of Mg and S (*25*, *29*, *43*, *46*) but the sudden depletion of Cl higher in the sequence (Fig. 4) (*29*).

The average 20 wt % SO_3 of the Burns formation corresponds to 480 kg of SO_3 in 1 m^3 of sediments (*81*). For simplicity of calculation, we assume that the groundwater has 1 g/liter of SO_3, surface water also has 1 g/liter of SO_3 (pH is around 3 if all S is from sulfuric acid), and the porosity of the sediments is 35% (*82*) at Meridiani. If the voids of the sediments are occupied by water and water ice, 350 liters of fluid with 1 g/liter of SO_3 can precipitate 0.35 kg of SO_3 at most in 1 m^3 of sediments for each freeze-thaw cycle. Therefore, to accumulate 20 wt % SO_3 (4.8×10^2 kg of SO_3/m^3) within the seasonal frozen zone, it requires ~1.37×10^4 to 10^5 ($= 4.8 \times 10^2/0.35$) seasonal freeze-thaw cycles. The estimate is the least value because the porosity of the sediments increases gradually to 35% with freeze-thaw cycles, and some sulfur can be leached downward during the thawing stage.

Formation of ferric concretions

Nano-sized Fe oxides coated on sand particles can be partly dissolved by low-pH water, which accounts for the bleaching (*89*) of the upper units of the Burns and Grasberg formations. Freezing can further induce aggregation of Fe oxides to form coarse specular grains (*38*, *54*, *83*), the thermal emission spectra of which are consistent with those of the average thermal emission spectrometry (TES) spectrum and mini-TES spectrum from Meridiani Planum (*38*). The oxidation of the ferrous iron in the upward migrating groundwater by the oxidants (e.g., chlorate) dissolved in surface water can promote the formation of hematite. Fe oxides tend to be enriched just below the bleaching zone (Fig. 1A), possibly because hematite precipitation is favored under a slightly acidic environment compared to jarosite and groundwater accumulated just below the frozen front can dilute acidity enhanced by surface freezing. Some hematite can also be formed by the decomposition of jarosite formed during the freezing period owing to the change in pH and salinity of fluids (*32*, *84*) during the thawing period. The hematite spherules have been hypothesized to form owing to the cycling of upward-migrating groundwater and oxidation of aqueous Fe^{2+} during seasonal freeze-thaw (Fig. 5F) (*37*). The well-drained environment of martian sediments with high porosity can account for the spherical shape of the Fe concretions (*85*).

Freeze-thaw and cryosuction as a fundamental process on Mars

On Hesperian Mars, the intersecting regions with high surface temperature and shallow water table, which allow for seasonal freeze-thaw resulting in upward migration of groundwater via cryosuction, provide a viable mechanism for the formation of layered sulfate-rich sediments. The higher temperatures at low latitudes during the Hesperian allowing cyclical thawing may explain why most of the hydrated sulfates on Mars are concentrated in the interior layered deposits of Valles Marineris chasmata systems and layered rocks in Aram Chaos, Arabia Terra, and Meridiani Planum (*14*, *15*).

A global groundwater table/upwelling scenario is not necessarily required in the cryosuction/freeze-thaw model. Local sources of snowmelt can be wicked up into mounds of eolian deposits (*5*), which could explain the occurrence of sulfate settings such as the interior layered deposits (*14*, *15*). It is possible that some of the sulfate-rich layered deposits in Gale crater also could have been formed by the freeze-thaw cycles. As Curiosity ascends through the layered mound sediments in the coming years, these hypotheses are testable with mineralogical, chemical, and textural observations (e.g., high porosity, the platy structure with abundant coarse planar voids but little fine voids, and the upper bleaching and brecciated zone and lower darker and less brecciated zone with sudden horizontal boundary in a meter-scale section) from the rover.

Although most layered sulfates appear in low-elevation regions (*13*), the layered sulfates are distributed over a range of elevations and contexts (*5*). The concept of a global groundwater table and predicted upwelling regions might not well explain the layered sulfates that occur in areas with high elevations. However, observations from the Qaidam Basin, a high-elevation desert in western China (fig. S1), illustrate the importance of local and regional glacier melt in recharging shallow groundwater (*39*). On Mars, it should be expected that similar, disconnected shallow groundwater settings fed by local and regional recharge should have been common. Meltwater of snow in higher elevations could have efficiently recharged the local or regional shallow groundwater.

The average temperature during the formation of the sulfate-rich deposits should have been at or just below the freezing point of liquid water in the equatorial region. It suggests a cold climate with a global average temperature below 0°C during the Hesperian. The model provides an unearthly but simple mechanism through which vast, thick, intensely altered but largely homogeneous sulfate-rich rocks could have formed on Mars, and it highlights the possible importance of freeze-thaw as a mechanism of chemical weathering on the red planet.

MATERIALS AND METHODS

The concentrations of element oxides were obtained with the APXS on board the Opportunity rover. A description of the instrument, calibration methods, and data quantification can be found in the study of Gellert *et al.* (*86*). Data were downloaded via the PDS Geosciences node (see Data and materials availability below). The APXS is a contact instrument that uses curium-244 sources to induce particle-induced x-ray emission and x-ray fluorescence. The APXS spectra represent the average composition over the sampled area, which is 38 mm in diameter when the instrument is in contact with the sample.

Supplementary Materials

This PDF file includes:

Figs. S1 to S3

REFERENCES AND NOTES

1. A. M. Annex, K. W. Lewis, Regional correlations in the layered deposits of arabia terra, Mars. *J. Geophys. Res. Planets* **125**, e06188 (2020).
2. S. Murchie, L. Roach, F. Seelos, R. Milliken, J. Mustard, R. Arvidson, S. Wiseman, K. Lichtenberg, J. Andrews-Hanna, J. Bishop, J. P. Bibring, M. Parente, R. Morris, Evidence for the origin of layered deposits in Candor Chasma, Mars, from mineral composition and hydrologic modeling. *J. Geophys. Res.* **114**, E00D05 (2009).
3. L. LeDeit, S. LeMouélic, O. Bourgeois, J. P. Combe, D. Mège, C. Sotin, A. Gendrin, E. Hauber, N. Mangold, J. P. Bibring, Ferric oxides in East Candor Chasma, Valles Marineris (Mars) inferred from analysis of OMEGA/Mars Express data: Identification and geological interpretation. *J. Geophys. Res.* **113**, E07001 (2008).
4. J. W. Head, L. Wilson, Sulfates on Mars: A pyroclastic airfall model for origin, emplacement, and initial alteration of Valles Marineris interior layered deposits (ILD), in *52nd Lunar and Planetary Science Conference*. LPI, 2048, 4 to 8 May 2020.
5. J. Michalski, P. B. Niles, Atmospheric origin of martian interior layered deposits: Links to climate change and the global sulfur cycle. *Geology* **40**, 419–422 (2012).
6. K. W. Lewis, O. Aharonson, J. P. Grotzinger, R. L. Kirk, A. S. McEwen, T. A. Suer, Quasi-periodic bedding in the sedimentary rock record of mars. *Science* **322**, 1532–1535 (2008).
7. K. W. Lewis, O. Aharonson, Occurrence and origin of rhythmic sedimentary rocks on Mars. *J. Geophys. Res.* **119**, 1432–1457 (2014).
8. P. B. Niles, J. Michalski, Meridiani Planum sediments on mars formed through weathering in massive ice deposits. *Nat. Geosci.* **2**, 215–220 (2009).
9. J. R. Michalski, T. A. Goudg, J. Cuadros, J. Mustard, S. S. Johnson, L. Xiao, Geological diversitiy and microbiological potential of lakes on Mars. *Nat. Astron.* **6**, 1133–1141 (2022).
10. T. A. Goudge, J. W. Head, J. F. Mustard, C. I. Fassett, An analysis of open-basin lake deposits on Mars: Evidence for the nature of associated lacustrine deposits and post-lacustrine modification processes. *Icarus* **219**, 211–229 (2012).
11. T. A. Goudge, K. L. Aureli, J. W. Head, C. I. Fassett, J. F. Mustard, Classification and analysis of candidate impact crater-hosted closed-basin lakes on Mars. *Icarus* **260**, 346–367 (2015).
12. Y. Langevin, F. Poulet, J.-P. Bibring, B. Gondet, Sulfates in the north polar region of Mars detected by OMEGA/Mars Express. *Science* **307**, 1584–1586 (2005).
13. E. S. Kite, I. Halevy, M. A. Kahre, M. J. Wolff, M. Manga, Seasonal melting and the formation of sedimentary rocks on Mars, with predictions for the Gale Crater mound. *Icarus* **223**, 181–210 (2013).
14. A. Gendrin, N. Mangold, J. P. Bibring, Y. Langevin, B. Gondet, F. Poulet, G. Bonello, C. Quantin, J. Mustard, R. Arvidson, S. LeMouélic, Sulfates in Martian layered terrains: The OMEGA/Mars express view. *Science* **307**, 1587–1591 (2005).
15. Y. Liu, T. A. Goudge, J. G. Catalano, A. Wang, Spectral and stratigraphic mapping of hydrated minerals associated with interior layered deposits near the southern wall of Melas Chasma, Mars. *Icarus* **302**, 62–79 (2018).
16. B. M. Hynek, R. E. Arvidson, R. J. Phillips, Geologic setting and origin of Terra Meridiani hematite deposit on Mars. *J. Geophys. Res. Planets* **107**, 5088 (2002).
17. P. R. Christensen, J. L. Bandfield, R. N. Clark, K. S. Edgett, V. E. Hamilton, T. Hoefen, H. H. Kieffer, R. O. Kuzmin, M. D. Lane, M. C. Malin, Detection of crystalline hematite mineralization on Mars by the Thermal Emission Spectrometer: Evidence for near-surface water. *J. Geophys. Res. Planets* **105**, 9623–9642 (2000).
18. P. R. Christensen, S. W. Ruff, Formation of the hematite-bearing unit in Meridiani Planum: Evidence for deposition in standing water. *J. Geophys. Res. Planets* **109**, E08003 (2004).
19. S. W. Squyres, J. P. Grotzinger, R. E. Arvidson, J. F. Bell, W. Calvin, P. R. Christensen, B. C. Clark, J. A. Crisp, W. H. Farrand, K. E. Herkenhoff, In situ evidence for an ancient aqueous environment at Meridiani Planum, Mars. *Science* **306**, 1709–1714 (2004).
20. S. W. Squyres, A. H. Knoll, R. E. Arvidson, J. W. Ashley, J. F. Bell, W. M. Calvin, P. R. Christensen, B. C. Clark, B. A. Cohen, P. A. DeSouza, Exploration of Victoria crater by the Mars rover Opportunity. *Science* **324**, 1058–1061 (2009).
21. S. W. Squyres, A. H. Knoll, R. E. Arvidson, B. C. Clark, J. P. Grotzinger, B. L. Jolliff, S. M. McLennan, N. Tosca, J. F. Bell, W. M. Calvin, Two years at Meridiani Planum: Results from the Opportunity Rover. *Science* **313**, 1403–1407 (2006).
22. J. C. Andrews-Hanna, M. T. Zuber, R. E. Arvidson, S. M. Wiseman, Early Mars hydrology: Meridiani playa deposits and the sedimentary record of Arabia Terra. *J. Geophys. Res. Planets* **115**, E06002 (2010).
23. J. C. Andrews-Hanna, R. J. Phillips, M. T. Zuber, Meridiani Planum and the global hydrology of Mars. *Nature* **446**, 163–166 (2007).
24. J. P. Grotzinger, R. E. Arvidson, J. F. Bell, W. Calvin, B. C. Clark, D. A. Fike, M. Golombek, R. Greeley, A. Haldemann, K. E. Herkenhoff, B. L. Jolliff, A. H. Knoll, M. Malin, S. M. McLennan, T. Parker, L. Soderblom, J. N. Sohl-Dickstein, S. W. Squyres, N. J. Tosca, W. A. Watters, Stratigraphy and sedimentology of a dry to wet eolian depositional system, Burns formation, Meridiani Planum, Mars. *Earth Planet. Sci. Lett.* **240**, 11–72 (2005).
25. R. Amundson, Meteoric water alteration of soil and landscapes at Meridiani Planum, Mars. *Earth Planet. Sci. Lett.* **488**, 155–167 (2018).
26. L. P. Knauth, D. M. Burt, K. H. Wohletz, Impact origin of sediments at the opportunity landing site on Mars. *Nature* **438**, 1123–1128 (2005).
27. B. M. Hynek, Implications for hydrologic processes on Mars from extensive bedrock outcrops throughout Terra Meridiani. *Nature* **431**, 156–159 (2004).
28. T. M. McCollom, B. M. Hynek, A volcanic environment for bedrock diagenesis at Meridiani Planum on Mars. *Nature* **438**, 1129–1131 (2005).
29. B. C. Clark, R. V. Morris, S. M. McLennan, R. Gellert, B. Jolliff, A. H. Knoll, S. W. Squyres, T. K. Lowenstein, D. W. Ming, N. J. Tosca, A. Yen, P. R. Christensen, S. Gorevan, J. Brückner, W. Calvin, G. Dreibus, W. Farrand, G. Klingelhoefer, H. Waenke, J. Zipfel, J. F. Bell, J. Grotzinger, H. Y. McSween, R. Rieder, Chemistry and mineralogy of outcrops at Meridiani Planum. *Earth Planet. Sci. Lett.* **240**, 73–94 (2005).
30. P. B. Niles, J. Michalski, D. W. Ming, D. C. Golden, Elevated olivine weathering rates and sulfate formation at cryogenic temperatures on Mars. *Nat. Commun.* **8**, 998 (2017).
31. N. J. Tosca, S. M. McLennan, B. C. Clark, J. P. Grotzinger, J. A. Hurowitz, A. H. Knoll, C. Schröder, S. W. Squyres, Geochemical modeling of evaporation processes on Mars: Insight from the sedimentary record at Meridiani Planum. *Earth Planet. Sci. Lett.* **240**, 122–148 (2005).
32. S. M. McLennan, J. F. Bell III, W. M. Calvin, P. R. Christensen, B. C. Clark, P. A. de Souza, J. Farmer, W. H. Farrand, D. A. Fike, R. Gellert, A. Ghosh, T. D. Glotch, J. P. Grotzinger, B. Hahn, K. E. Herkenhoff, J. A. Hurowitz, J. R. Johnson, S. S. Johnson, B. Jolliff, G. Klingelhöfer, A. Yen, Provenance and diagenesis of the evaporite-bearing Burns formation, Meridiani Planum, Mars. *Earth Planet. Sci. Lett.* **240**, 95–121 (2005).
33. E. S. Kite, M. Melwani Daswani, Geochemistry constrains global hydrology on Early Mars. *Earth Planet. Sci. Lett.* **524**, 115718 (2019).
34. A. Zandanel, R. Hellmann, L. Truche, V. Roddatis, M. Mermoux, G. Choblet, G. Tobie, Geologically rapid aqueous mineral alteration at subfreezing temperatures in icy worlds. *Nat. Astron.* **6**, 554–559 (2022).
35. G. Baccolo, B. Delmonte, P. B. Niles, G. Cibin, E. DiStefano, D. Hampai, L. Keller, V. Maggi, A. Marcelli, J. Michalski, C. Snead, M. Frezzotti, Jarosite formation in deep Antarctic ice provides a window into acidic, water-limited weathering on Mars. *Nat. Commun.* **12**, 436 (2021).
36. D. Zhang, W. Shijie, Mechanism of freeze-thaw action in the process of soil salinization in northeast China. *Environ. Geol.* **41**, 96–100 (2001).
37. Q. Wang, Z. Jiang, Z. Sun, Distribution and formation environment of Fe-Mn nodules in soil derived from Quaternary loess in north China. *Acta Pedofil. Sin.* **56**, 288–293 (2019).
38. A. S. Madden, V. E. Hamilton, M. E. E. Madden, P. R. Larson, M. A. Miller, Low-temperature mechanism for formation of coarse crystalline hematite through nanoparticle aggregation. *Earth Planet. Sci. Lett.* **298**, 377–384 (2010).

39. Y. Xiao, J. Shao, S. K. Frape, Y. Cui, X. Dang, S. Wang, Y. Ji, Groundwater origin, flow regime and geochemical evolution in arid endorheic watersheds: A case study from the Qaidam Basin, northwestern China. *Hydrol. Earth Syst. Sci.* **22**, 4381–4400 (2018).
40. W. Cheng-hai, D. Wen-jie, W. Zhi-gang, Anomaly feature of seasonal frozen soil variations on the Qinghai-Tibet Plateau. *J. Geogr. Sci.* **12**, 99–107 (2002).
41. J. C. Stuurop, S. E. A. T. M. van der Zee, C. I. Voss, H. K. French, Simulating water and heat transport with freezing and cryosuction in unsaturated soil: Comparing an empirical, semi-empirical and physically-based approach. *Adv. Water Resour.* **149**, 103846 (2021).
42. S. W. Squyres, A. H. Knoll, Sedimentary rocks at Meridiani Planum: Origin, diagenesis, and implications for life on Mars. *Earth Planet. Sci. Lett.* **240**, 1–10 (2005).
43. T. M. McCollom, Geochemical trends in the burns formation layered sulfate deposits at Meridiani Planum, Mars, and implications for their origin. *J. Geophys. Res. Planets* **123**, 2393–2429 (2018).
44. D. W. Mittlefehldt, R. Gellert, B. von Bommel, D. W. Ming, A. S. Yen, B. C. Clark, R. V. Morris, C. Schröder, L. S. Crumpler, J. A. Grant, B. L. Jolliff, R. E. Arvidson, W. H. Farrand, K. E. Herkenhoff, C. M. Schrader, J. W. Rice, Diverse lithologies and alteration events on the rim of Noachian-aged endeavour crater, Meridiani Planum, Mars: In situ compositional evidence. *J. Geophys. Res. Planets* **123**, 1255–1306 (2018).
45. D. W. Mittlefehldt, R. Gellert, S. Van Bommel, R. E. Arvidson, J. W. Ashley, B. C. Clark, L. S. Crumpler, W. H. Farrand, M. P. Golombek, J. A. Grant, R. V. Morris, C. Schröder, Geology and geochemistry of noachian bedrock and alteration events, Meridiani Planum, Mars: MER opportunity observations. *J. Geophys. Res. Planets* **126**, e06915 (2021).
46. T. M. McCollom, B. Hynek, Geochemical data indicate highly similar sediment compositions for the Grasberg and Burns formations on Meridiani Planum, Mars. *Earth Planet. Sci. Lett.* **557**, 116729 (2021).
47. G. Kocurek, J. Nielson, Conditions favourable for the formation of warm-climate aeolian sand sheets. *Sedimentology* **33**, 795–816 (1986).
48. S. W. Squyres, R. E. Arvidson, J. F. Bell, F. Calef, B. C. Clark, B. A. Cohen, L. A. Crumpler, P. A. DeSouza, W. H. Farrand, R. Gellert, Ancient impact and aqueous processes at Endeavour Crater Mars. *Science* **336**, 570–576 (2012).
49. B. M. Hynek, R. J. Phillips, The stratigraphy of Meridiani Planum, Mars, and implications for the layered deposits' origin. *Earth Planet. Sci. Lett.* **274**, 214–220 (2008).
50. H. Yoshida, H. Hasegawa, N. Katsuta, I. Maruyama, S. Sirono, M. Minami, Y. Asahara, S. Nishimoto, Y. Yamaguchi, N. Ichinnorov, R. Metcalfe, Fe-oxide concretions formed by interacting carbonate and acidic waters on Earth and Mars. *Sci. Adv.* **4**, eaau0872 (2018).
51. R. C. Peterson, R. Wang, Crystal molds on Mars: Melting of a possible new mineral species to create Martian chaotic terrain. *Geology* **34**, 957–960 (2006).
52. R. C. Peterson, W. Nelson, B. Madu, H. F. Shurvell, Meridianiite: A new mineral species observed on Earth and predicted to exist on Mars. *Am. Mineral.* **92**, 1756–1759 (2007).
53. B. Van Vliet-Lanoë, Frost effects in soils. *Soils Quat. Landsc. Evol.* **117**, 158 (1985).
54. Z. Zhang, M. A. Wei, F. Wenjie, X. Donghui, H. O. U. Xin, Reconstruction of soil particle composition during freeze-thaw cycling: A review. *Pedosphere* **26**, 167–179 (2016).
55. I. A. Taina, R. J. Heck, W. Deen, E. Y. T. Ma, Quantification of freeze–thaw related structure in cultivated topsoils using X-ray computer tomography. *Can. J. Soil Sci.* **93**, 533–553 (2013).
56. M. Ghazavi, M. Roustaei, Freeze–thaw performance of clayey soil reinforced with geotextile layer. *Cold Reg. Sci. Technol.* **89**, 22–29 (2013).
57. S. Taber, The mechanics of frost heaving. *J. Geol.* **38**, 303–317 (1930).
58. T. M. McCollom, B. M. Hynek, Proposed Origin of the Burns Formation (Meridiani Planum, Mars) by Erosion, Reworking, and Diagenetic Alteration of a Grasberg-Like Precursor. *J. Geophys. Res. Planets* **128**, e2022JE007374 (2023).
59. J. Liu, J. R. Michalski, M.-F. Zhou, Intense subaerial weathering of eolian sediments in Gale crater, Mars. *Sci. Adv.* **7**, eabh2687 (2021).
60. A. H. Hofstra, Characteristics and models for Carlin-type gold deposits. *Rev. Econ. Geol.* **13**, 163–220 (2000).
61. S. E. Kesler, J. Fortuna, Z. Ye, J. C. Alt, D. P. Core, P. Zohar, J. Borhauer, S. L. Chryssoulis, Evaluation of the role of sulfidation in deposition of gold, Screamer section of the Betze-Post Carlin-type Deposit, Nevada. *Econ. Geol.* **98**, 1137–1157 (2003).
62. J. A. Hurowitz, S. M. McLennan, A ~ 3.5 Ga record of water-limited, acidic weathering conditions on Mars. *Earth Planet. Sci. Lett.* **260**, 432–443 (2007).
63. G. Klingelhöfer, R. Van Morris, B. Bernhardt, C. Schröder, D. S. Rodionov, P. A. DeSouza, A. Yen, R. Gellert, E. N. Evlanov, B. Zubkov, Jarosite and hematite at Meridiani Planum from Opportunity's Mössbauer spectrometer. *Science* **306**, 1740–1745 (2004).
64. E. K. Gibson, S. J. Wentworth, D. S. McKay, Chemical weathering and diagenesis of a cold desert soil from Wright Valley, Antarctica: An analog of Martian weathering processes. *J. Geophys. Res. Solid Earth.* **88**, A912–A928 (1983).
65. B. Sutter, J. B. Dalton, S. A. Ewing, R. Amundson, C. P. McKay, Terrestrial analogs for interpretation of infrared spectra from the Martian surface and subsurface: Sulfate, nitrate, carbonate, and phyllosilicate-bearing Atacama Desert soils. *J. Geophys. Res. Biogeo.* **112**, (2007).
66. J. A. Hurowitz, S. M. McLennan, A ~3.5 Ga record of water-limited, acidic weathering conditions on Mars. *Earth Planet. Sci. Lett.* **260**, 432–443 (2007).
67. J. Liu, J. R. Michalski, M.-F. Zhou, Intense subaerial weathering of eolian sediments in Gale crater, Mars. *Sci. Adv.* **7**, eabh2687 (2021).
68. T. S. Peretyazhko, P. B. Niles, B. Sutter, R. V. Morris, D. G. Agresti, L. Le, D. W. Ming, Smectite formation in the presence of sulfuric acid: Implications for acidic smectite formation on early Mars. *Geochim. Cosmochim. Acta* **220**, 248–260 (2018).
69. J. A. Hurowitz, W. W. Fischer, N. J. Tosca, R. E. Milliken, Origin of acidic surface waters and the evolution of atmospheric chemistry on early Mars. *Nat. Geosci.* **3**, 323–326 (2010).
70. Y. Y. S. Zhao, S. M. McLennan, W. A. Jackson, S. Karunatillake, Photochemical controls on chlorine and bromine geochemistry at the Martian surface. *Earth Planet. Sci. Lett.* **497**, 102–112 (2018).
71. Z. Wu, A. Wang, W. M. Farrell, Y. Yan, K. Wang, J. Houghton, A. W. Jackson, Forming perchlorates on Mars through plasma chemistry during dust events. *Earth Planet. Sci. Lett.* **504**, 94–105 (2018).
72. S.-Y. Qu, Y.-Y. S. Zhao, H. Cui, X.-Z. Yin, W. A. Jackson, X. Nie, Z.-C. Wu, J.-H. Wang, D.-S. Zhou, C. Qi, X.-Y. Li, J.-Z. Liu, Preferential formation of chlorate over perchlorate on Mars controlled by iron mineralogy. *Nat. Astron.* **6**, 436–441 (2022).
73. K. Mitra, J. G. Catalano, Chlorate as a potential oxidant on Mars: Rates and products of dissolved Fe (II) oxidation. *J. Geophys. Res. Planets* **124**, 2893–2916 (2019).
74. E. Sefton-Nash, D. C. Catling, Hematitic concretions at Meridiani Planum, Mars: Their growth timescale and possible relationship with iron sulfates. *Earth Planet. Sci. Lett.* **269**, 366–376 (2008).
75. K. Mitra, E. L. Moreland, A. L. Knight, J. G. Catalano, Rates and products of iron oxidation by chlorate at low temperatures (0 to 25°C) and implications for Mars geochemistry. *ACS Earth Space Chem.* **6**, 250–260 (2022).
76. R. Chang, Y. Zhao, Partitioning behavior of Br and Cl during jarosite precipitation and its implications for sedimentary rock on Mars. *Chin. Sci. Bull.* **63**, 461–470 (2018).
77. G. B. Alexander, W. M. Heston, R. K. Iler, The solubility of amorphous silica in water. *J. Phys. Chem.* **58**, 453–455 (1954).
78. W. L. Marshall, J. M. Warakomski, Amorphous silica solubilities—II. Effect of aqueous salt solutions at 25 C. *Geochim. Cosmochim. Acta* **44**, 915–924 (1980).
79. H.-Y. Xie, X.-W. Jiang, S.-C. Tan, L. Wan, X.-S. Wang, S.-H. Liang, Y. Zeng, Interaction of soil water and groundwater during the freezing–thawing cycle: Field observations and numerical modeling. *Hydrol. Earth Syst. Sci.* **25**, 4243–4257 (2021).
80. X. Wang, Y. Sara Zhao, D. R. Hood, S. Karunatillake, D. Laczniak, M. E. Schmidt, M. Vithanage, Multiphase Volatilization of Halogens at the Soil-Atmosphere Interface on Mars. *J. Geophys. Res. Planets* **126**, e06929 (2021).
81. B. M. Hynek, T. M. McCollom, A. Szynkiewicz, Sulfur cycling and mass balance at Meridiani, Mars. *Geophys. Res. Lett.* **46**, 11728–11737 (2019).
82. J. R. Michalski, T. C. Onstott, S. J. Mojzsis, J. Mustard, Q. H. S. Chan, P. B. Niles, S. S. Johnson, The Martian subsurface as a potential window into the origin of life. *Nat. Geosci.* **11**, 21–26 (2018).
83. M. R. Sexton, M. E. E. Madden, A. L. Swindle, V. E. Hamilton, B. R. Bickmore, A. S. E. Madden, Considering the formation of hematite spherules on Mars by freezing aqueous hematite nanoparticle suspensions. *Icarus* **286**, 202–211 (2017).
84. V. Barrón, J. Torrent, J. P. Greenwood, Transformation of jarosite to hematite in simulated martian brines. *Earth Planet. Sci. Lett.* **251**, 380–385 (2006).
85. W. R. Phillippe, R. L. Blevins, R. I. Barnhisel, H. H. Bailey, Distribution of concretions from selected soils of the inner bluegrass region of Kentucky. *Soil Sci. Soc. Am. J.* **36**, 171–173 (1972).
86. R. Gellert, R. Rieder, J. Brückner, B. C. Clark, G. Dreibus, G. Klingelhöfer, G. Lugmair, D. W. Ming, H. Wänke, A. Yen, Alpha particle x-ray spectrometer (APXS): Results from Gusev crater and calibration report. *J. Geophys. Res. Planets* **111**, (2006).
87. S. R. Taylor, S. McLennan, *Planetary Crusts: Their Composition, Origin and Evolution* (Cambridge Univ. Press, 2009), vol. 10.
88. W. P. Dunlap, N. C. Silver, Confidence intervals and standard errors for ratios of normal variables. *Behav. Res. Meth. Instr. Comput.* **18**, 469–471 (1986).
89. R. Gellert, MER APXS derived oxide data bundle. *NASA Planet. Data Syst.* (2019).

Acknowledgments: We are very grateful to those Opportunity team members and Opportunity project's engineering and management teams. We thank Z. Asimaki for providing sample classification, X. Zhang for the discussion, and P. Nile for insightful comments. We are grateful for the assistance provided by L. Liu, J. Guan, Y. Yao, and J. Xu during field trips. J.L. would also like to acknowledge his wife (W. Shen) for persistent curiosity and fundamental questions that have contributed to the establishment and development of the model. We would also like to acknowledge Shenzhen Institute of Research and Innovation, the University of Hong Kong for managing the NSFC project funded for J.L. **Funding:** This work was funded by the Research Grants Council General Research Fund to J.R.M. (grant number 17311022) and J.L. (grant number 17306623) and the National Science Foundation of China to J.L. (grant number 42241129). **Author**

contributions: Conceptualization: J.L. and J.R.M. Methodology: J.L. and J.R.M. Investigation: J.L. and J.R.M. Visualization: J.L., W.G., and J.R.M. Supervision: J.R.M. Writing—original draft: J.L. and J.R.M. Writing—review and editing: J.R.M., W.G., C.S., Y.L.-L. Validation: C.S. and Y.L.-L. Funding acquisition: J.R.M. Project administration: J.R.M. **Competing interests:** The authors declare that they have no competing interests. **Data and materials availability:** All data needed to evaluate the conclusions in the paper are present in the paper and/or the Supplementary Materials. Data for APXS integrations on all rock and soil targets acquired by Opportunity through Sol 5105 are available on the publicly accessible NASA Planetary Data System (*89*).

Submitted 8 April 2023
Accepted 19 December 2023
Published 17 January 2024
10.1126/sciadv.adi1805

ScienceAdvances

Freeze-thaw cycles drove chemical weathering and enriched sulfates in the Burns formation at Meridiani, Mars

Jiacheng Liu, Joseph R. Michalski, Wenyuan Gao, Christian Schröder, and Yi-Liang Li

Sci. Adv. **10** (3), eadi1805. DOI: 10.1126/sciadv.adi1805

Science Advances (ISSN 2375-2548) is published by the American Association for the Advancement of Science. 1200 New York Avenue NW, Washington, DC 20005. The title *Science Advances* is a registered trademark of AAAS.